J|A|C|S
ARTICLES
Published on Web 02/27/2002

Deuterium Structural Effects in Inorganic and Bioinorganic Aggregates

Jaeho Lee,[†] N. Dennis Chasteen,[‡] Guanghua Zhao,[‡]
Georgia C. Papaefthymiou,[§] and Sergiu M. Gorun*,[†]

Contribution from the Department of Chemistry, Brown University, Providence, Rhode Island 02912, Department of Chemistry, University of New Hampshire, Durham, New Hampshire 03824, and Department of Physics, Villanova University, Villanova, Pennsylvania 19085

Received June 12, 2001. Revised Manuscript Received November 30, 2001

Abstract: Deuterium kinetic isotope effects are widely used in chemical and biological research. Deuterium thermodynamic effects on the aqueous synthesis of inorganic materials, however, seem not to have been recognized. Here we report that the simple replacement of H_2O with D_2O in the synthesis of a solid-state manganese complex results in a new structurally and magnetically distinct phase. When iron oxides are synthesized, the relative amount of the mineral phases obtained in H_2O vs D_2O is different. The morphology and magnetic properties of the iron core of the iron storage protein ferritin are likewise different when mineralization is carried out in heavy water. The formation of extra inorganic solids, change in the ratio of two phases or alteration of a single phase morphology in D_2O suggest that new inorganic and bioinorganic metal complexes might be obtained by using the thermodynamic isotope effect.

Introduction and Background

Deuterium isotope effects are routinely used as mechanistic tools for kinetics studies and for structural determinations by magnetic resonance and neutron diffraction. Generally, deuterium substitution is thought to have a minimal effect on the structural organization and thermodynamic stability of *molecules* because of the similar energies of O−H and O−D bonds, which translates into hydrogen-bonded O···O distances varying by 0.03 Å or less.[1,2] However, the importance of small differences in hydrogen-bond strength to the *solid-state* structural organization of deuterated molecules seems to have been little recognized. Unlike covalent bonds, which have atom-pair properties, hydrogen bonds have group properties, their energy and geometry being a function of the global pattern of H-bonding in the solid. Thus, hydrogen-bond strength as well as packing forces, degree of solvation and ionic radii are factors determining the type of hydrogen-bonding network obtained for a particular material.

Differences in hydrogen-bond strength between H_2O and D_2O are reflected, *inter alia*, in the higher melting and boiling points, 3.82 and 101.42 °C, respectively, for D_2O. Moreover, the ion product ratio $K_w(H_2O)/K_w(D_2O) = 7.47 \pm 0.24$ at 25 °C reflects a smaller degree of dissociation of D_2O compared to H_2O.[3] As a consequence of differences in hydrogen bonding, ice IV is a structurally well-defined phase for D_2O, but not for H_2O.[4] There are also several examples where the physical properties of metal salts are affected by isotopic composition. Included among these are the altered Jahn−Teller distortions of copper Tutton salts,[5] $(NH_4)_2[Cu(H_2O)_6](SO_4)_2$, and shifts in ferro- or antiferroelectric transition temperatures of KH_2PO_4 upon deuteration.[6]

To our knowledge, there are no previous examples where H/D exchange has altered the lattice structure of a metal salt, producing a new solid-state material. Polynuclear metal aggregates with a large degree of hydration and/or numerous oxo/hydroxo groups are good candidates for isotopic effects on lattice structures because of the presence of extensive hydrogen-bonding networks in their solid-state supramolecular structures. Metal aggregates that form in aqueous solutions occupy a central position at the intersection of coordination complexes, solid-state materials and the biominerals found in nature; however, the influence of isotopic substitution on their structural properties has not been previously examined. The evolutionary-designed synthetic schemes in nature result in the reproducible synthesis of polynuclear materials such as magnetite in magnetotactic bacteria,[7,8] the oxo/hydroxo iron cores of the ferritins[9] and other important biominerals.[10] We have therefore undertaken a study of isotope effects on the solid-state architecture of some inorganic and bioinorganic aggregates. By way of three examples, we demonstrate that H/D isotopic structural effects

[†] Department of Chemistry, Brown University.
[‡] Department of Chemistry, University of New Hampshire.
[§] Department of Physics, Villanova University.

(1) Olovsson, I.; Jönsson, P.-G. In *The Hydrogen Bond*; Schuster, P., Zundel, G., Sandorfy, C., Eds.; North-Holland: Amsterdam, 1976.
(2) Gallagher, K. J. In *Hydrogen Bonding*; Hazi, D., Ed.; Pergamon Press: New York, 1959.
(3) Salomaa, P. *Acta Chem. Scand.* **1971**, *25*, 367.
(4) Whalley, E. In *The Hydrogen Bond*; Schuster, P., Zundel, G., Sandorfy, C., Eds.; North-Holland: Amsterdam, 1976.
(5) Henning, R. W.; Schultz, A. J.; Hitchman, M. A.; Kelly, G.; Astley, T. *Inorg. Chem.* **2000**, *39*, 765 and references therein.
(6) Ichikawa, M. *Ferroelectrics* **1995**, *168*, 177.
(7) Blakemore, R. P. *Annu. Rev. Microbiol.* **1982**, *36*, 217.
(8) Bazylinski, D. A.; Frankel, R. B.; Jannasch, H. W. *Nature* **1988**, *334*, 518.
(9) Chasteen, N. D.; Harrison, P. M. *J. Struct. Biol.* **1999**, *126*, 182 and references therein.
(10) Lowenstam, H. A. *Science* **1981**, *211*, 1126.

10.1021/ja011447q CCC: $22.00

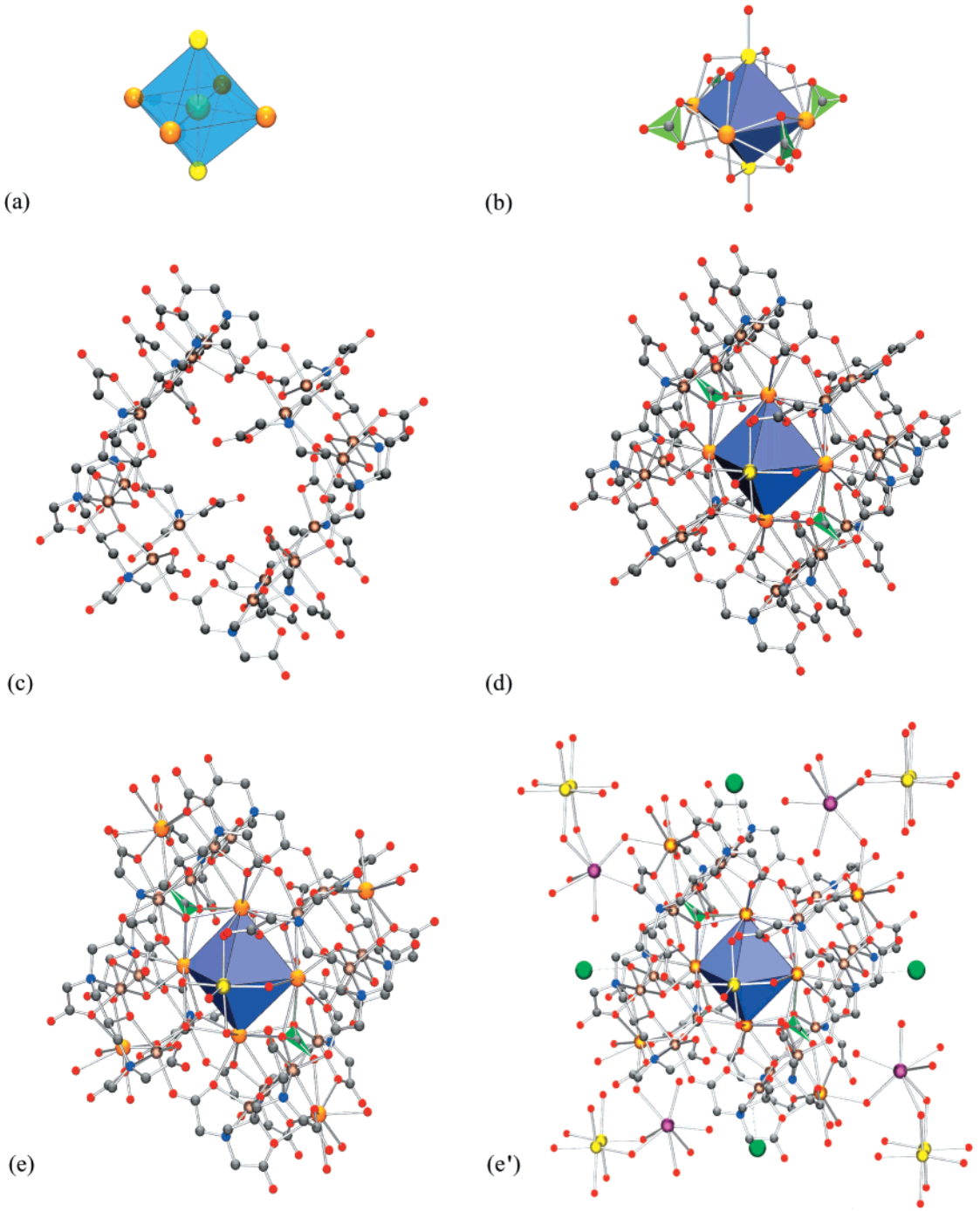

Figure 1. Stepwise construction of the Mn_{16} structures. Hydrogen atoms have been omitted for clarity. Color code: Cl, green; Ba, orange; Na, yellow; C, gray; O, red. (a) Central (μ_6-Cl)Ba_4Na_2 core, as a transparent octahedron; the Na−Cl−Na vector is along the 4-fold symmetry axis. (b) The carbonate-bridged (μ_6-Cl)$Ba_4Na_2(\mu$-$CO_3)_4(H_2O)_{10}$ kernel; the planar triangular carbonate ions are highlighted. (c) The $Mn_{16}L_8$ defined cavity with 4/*m* symmetry, viewed approximately along the 4-fold axis; color code: Mn, brown; N, blue. (d) The main-group elements central core and Mn−ligand structural assembly. (e) The H_2O phases, including four peripheral, solvated Ba^{2+} ions, common to both H_2O and D_2O phases. (e′) The D_2O phases, including two extra Cl^- (green), Na^+ (yellow), and Ba^{2+} (purple) ions disordered over four sites.

are manifested: (1) in the solid-state organization and magnetic properties of mixed-valent manganese(II,III) complexes crystallized from aqueous media, (2) in differing amounts of iron(III) oxide mineral phases produced from H_2O vs D_2O, and (3) in the magnetic properties of the nanoparticle core of the iron storage protein ferritin mineralized in H_2O vs D_2O buffers.

Results and Discussion

1. Isotope Effects on the Structures of Manganese Aggregate Complexes. Self-assembled manganese aggregates with significantly different solid-state structures and composition are produced (Table 1) when complexes of 1, 3-diamino-2-hydroxypropane-*N*,*N*,*N*′,*N*′-tetraacetic acid (H_5dhpta, L) are crystallized from H_2O vs D_2O solution under otherwise identical conditions (Experimental Section).

On average, the D_2O derived material **2** contains 2 additional Ba^{2+}, Na^+, and Cl^- ions, plus approximately 15−30 more water molecules than the H_2O derived material **1**. To verify that these materials can be obtained reproducibly, several structures were

Table 1. Synthesis, Composition, and Crystallographic Properties of $Mn_{16}O_m((O(H,D))_{8-m}(CO_3)_4L_8Ba_xNa_yCl_2 \bullet W((H,D)_2O)$ Phases[a,b]

	H_2O phases: **1a**, **b**,[11] **c**	D_2O phases: **2a**, **b**
reaction	$Mn(OAc)_2 + Ba^{2+} + L + NaCl \xrightarrow[H_2O,\ H_2O_2]{Na_2CO_3}$	$Mn(OAc)_2 + Ba^{2+} + L + NaCl \xrightarrow[D_2O,\ D_2O_2]{Na_2CO_3}$
	$Mn_{16}O_{8-m}(OH)_m(CO_3)_4L_8Ba_8Na_2Cl \bullet wH_2O$	$Mn_{16}O_{8-m}(OD)_m(CO_3)_4L_8Ba_{10\pm0.5}Na_{4\pm1}Cl_3 \bullet w'D_2O$
unit	**1a:** $a = b = 24.666(5)$ Å, $c = 21.257(7)$ Å	**2a**[d]**:** $a = b = 20.873(5)$ Å, $c = 27.085(6)$ Å
cells	$V = 12933(7)$ Å^3, $T = 298$ K; $w = 46$	$V = 11800(5)$ Å^3, $T = 293$ K, $w' = 82.6$
volumes	**1b:** $a = b = 25.091(9)$ Å, $c = 21.021(9)$ Å	**2a′**[e]**:** $a = b = 20.873(5)$ Å, $c = 27.085(6)$ Å
	$V = 13234(8)$ Å^3, $T = 298$ K, $w = \sim 53$	$V = 11800(5)$ Å^3, $T = 293$ K, $w' = 86.0$
	1c: $a = b = 25.320(2)$ Å, $c = 20.511(2)$ Å	**2b:** $a = b = 20.931(2)$ Å, $c = 26.858(3)$ Å
	$V = 13155(2)$ Å^3, $T = 173$ K, $w = \sim 61$	$V = 11767(2)$ Å^3, $T = 173$ K, $w' = 76$
space group	$I4/m$, $Z = 2$	$I4/m$, $Z = 2$
R[c],%	**1a:** 4.8; **1b:** 5.1; **1c:** 3.6	**2a:** 4.2; **2a′:** 5.3; **2b:** 4.2

[a] L = the pentaanion of 1, 3-diamino-2-hydroxypropane-*N*,*N*,*N*′,*N*′-tetraacetic acid. [b] The number of oxygen-bound D(H) atoms, number of cations, and the Mn ions valence are correlated. Due to the high, *I*4/*m* symmetry, the Mn oxidation state differences are not obvious from the single-crystal X-ray data. Four μ-OD deuterons of **2a** and **b** ($m = 4$) were found in difference Fourier maps and refined successfully (see the Supporting Information). [c] $R = \Sigma||F_o| - |F_c||/\Sigma|F_o|$, where F_o and F_c are the observed and calculated structure factors, respectively. [d] Refined on *F*. [e] Refined on F^2. See the Supporting Information for details.

determined on crystals from different sample preparations in H_2O (**1a**−**c**) and D_2O (**2a** and **b**) over the course of a two year period. **2a** and **2a′** are structures at 293 K of the same crystal obtained from D_2O, but refined by two different methods (see Table 1, footnotes d and e), whereas **2b** is a structure of a different crystal determined at 173 K.

Two complete structural determinations (**2a** and **b)** revealed a slight variability in the number of interstitial water molecules and in the amount of Ba^{2+} and Na^+ ions (different site occupancy factors), but this variability does not affect the overall structure of **2**. The same unit cell parameters were obtained on a number of other crystals of **2**, consistent with common structures for all. In **2**, the metal composition in Table 1, determined from site occupancies, corresponds well with the Mn_{16}:$Ba_{9.75}$:$Na_{3.5}$ ratio found by elemental analysis. The lattice D_2O molecules of **2** are highly disordered. The water content, 81.5 ± 5.5, was estimated both by X-ray refining the partial water occupancy (on *F* and F^2 for **2a** and **2a′**, respectively) and using the SQUEEZE function of PLATON.[12] The observed ±7% variability in the total number of water molecules reflects both the small differences in the data processing methods and the variability in the resultant degree of hydration in the synthesis of **2a** and **b**. Some variability in the water content of **1** among different crystals was also observed (Table 1).

Despite significantly different unit cells and compositions, **1** and **2** share some common structural features. A stepwise construction of *all* structures, starting from the geometrical center, begins with Figure 1a, b.

A common central core consists of a water-bridged octahedron of main group elements (equatorial Ba^{2+}, apical Na^+) that encapsulates a Cl^- ion. Carbonate ions bridge the equatorial Ba^{2+} ions, forming a $(\mu_6\text{-Cl})Ba_4Na_2(\mu\text{-}CO_3)_4((H,D)_2O)_{10}$ central unit (kernel). The sixteen $Mn^{2+,3+}$ ions, linked by the dhpta^{5-} pentaanion define a cavity with 4/*m* symmetry (Figure 1c) in which the $(\mu_6\text{-Cl})Ba_4Na_2(\mu\text{-}CO_3)_4(H,D_2O)_{10}$ kernel is formally inserted, resulting in the structure of Figure 1d.

The full structures of the H_2O phases are completed by four additional, hydrated Ba^{2+} ions, present also in the D_2O phases, located at the periphery of the $Mn_{16}L_8$ units and bonded to the ligand carbonyl groups as shown in Figure 1e.

The topologies of Figures 1a−e are preserved for the D_2O phase, but extra Ba^{2+}, Na^+ and Cl^- ions are located at the periphery of the $Mn_{16}L_8$ ring in this phase (Figure 1e′). The extra cations are no longer in direct contact with the ligand, but are linked by H-bonds formed by their D_2O of hydration. The number of these peripheral ions, as mentioned above, is slightly variable. The number of nonmagnetic Ba^{2+} and Na^+ cations, which correlates with the valence of the Mn ions and the ratio of the bridging oxo-hydroxo groups, might be expected to influence the architecture of the Mn ions and their ligands. The Mn_4 subunits, which generate the Mn_{16} aggregates by a 4-fold rotation, are very similar, however. The relevant Mn−Mn distances in the Mn_4 unit are summarized in Figure 2. While

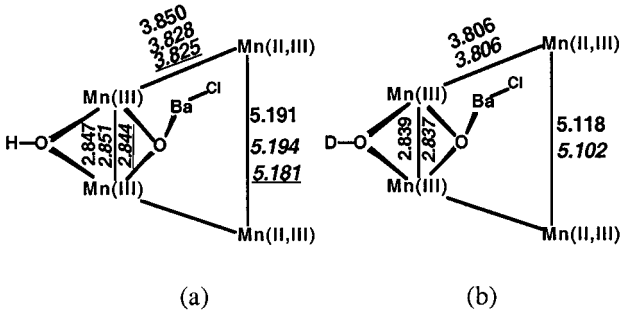

Figure 2. The Mn_4BaCl subsets (a): **1a**, **1b**, and **1c**. (b): **2a′** and **b**. The Mn−Mn distances for **1a**, **1b**, and **1c** are shown as stacked numbers in plain, italics, and underlined fonts style, respectively. The Mn−Mn distances for **2b** are in italics, below those for **2a**.

the distances are comparable for **1** and **2**, the values for the D_2O phase material are consistently shorter by 0.02−0.09 Å.

The two halves of each Mn_4 unit are symmetry related via a crystallographically imposed mirror plane that contains the two oxo groups and the Ba^{2+} and Cl^- ions. Based upon the Mn−ligand distances, charge considerations, and previously reported XAS data on **1b**,[11] two Mn sites are assigned as Mn(III) (average Mn−ligand bond lengths of 2.042, 2.032, 2.034, 2.035, and 2.036 Å for **1a**, **1b**, **1c**, **2a′**, and **2b**, respectively), whereas the other two are mixtures of Mn(II) and Mn(III). For the latter site, the average Mn−ligand bond distances are 2.227, 2.224, and 2.221 Å for **1a**, **1b**, and **1c**, and 2.223 and 2.224 Å, for **2a′** and **2b**, respectively. The X-ray and XAS data exclude higher Mn oxidation states. The Mn(III)−O(H,D) distances for **1a**, **1b**, **1c**, **2a′**, and **2b** are similar: 1.973(7), 2.032(8), 1.969(3), 1.956(5), and 1.963(3) Å, respectively. The corresponding

(11) (a) Grush, M. M.; Chan, J.; Stemmler, T. L.; George, S. J.; Ralston, C. Y.; Stibrany, R. T.; Gelasco, A. G.; Christou, G.; Gorun, S. M.; Penner-Hahn, J. E.; Cramer, S. P. *J. Am. Chem. Soc.* **1996**, *118*, 65. (b) Gorun, S. M.; Stibrany, R. T. *U.S. Patent* 5,099,045.
(12) Spek, A. L. *Acta Crystallogr.* **1990**, *A46*, C34.

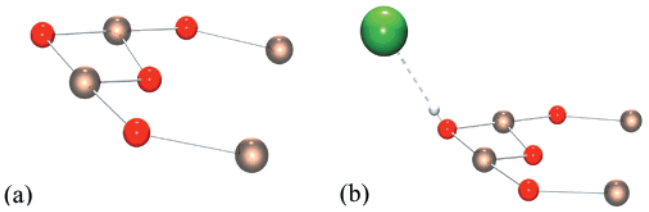

Figure 3. The Mn_4 subunits. (a) Mn_4 subunit of **1a**−**c**; hydrogen atoms have been omitted. (b) Mn_4Cl subunit of **2a** and **b**; the small sphere represents the Cl-bonded deuteron. Bond distances and angles for **2a** and **2b**: O···Cl: 3.095(8), 3.110(4) Å; O−H···Cl: 178(9)°, 165(8)°, respectively.

Mn−O−Mn angles, 92.4(4), 92.9(4), 92.5(2), 93.0(3), and 92.5(3)°, are virtually identical. The parameters of the Mn−O(Ba)−Mn sets are also similar: Mn−O = 1.829(6), 1.832(5), 1.841(3), 1.830(4), and 1.843(3) Å, respectively, while Mn−O−Mn angles are 102.1(5), 102.2(4), 101.1(2), 102.3(3), and 101.4(2)°, respectively. Thus, the architecture of the Mn_4 subset (and hence that of Mn_{16} units) is not changed appreciably by the isotopic substitution, but the slightly longer Mn(III)−OH distance for **1b** might indicate some Mn(II) admixture in its Mn(III) site. In addition to the extra Ba^{2+} and Na^+ cations, the switch to D_2O results in the incorporation of additional Cl^- anions, Figure 3.

Confirmation of the presence of the deuteron H-bonded to the extra Cl^-, as shown in Figure 3b, was sought by a survey[13] of known inorganic μ-oxo-H···Cl^- contacts up to 3.6 Å, the limit of the sum of the Allinger[14] van der Waals radii of oxygen and chloride. The 23 O···Cl contacts, roughly defining a bell-

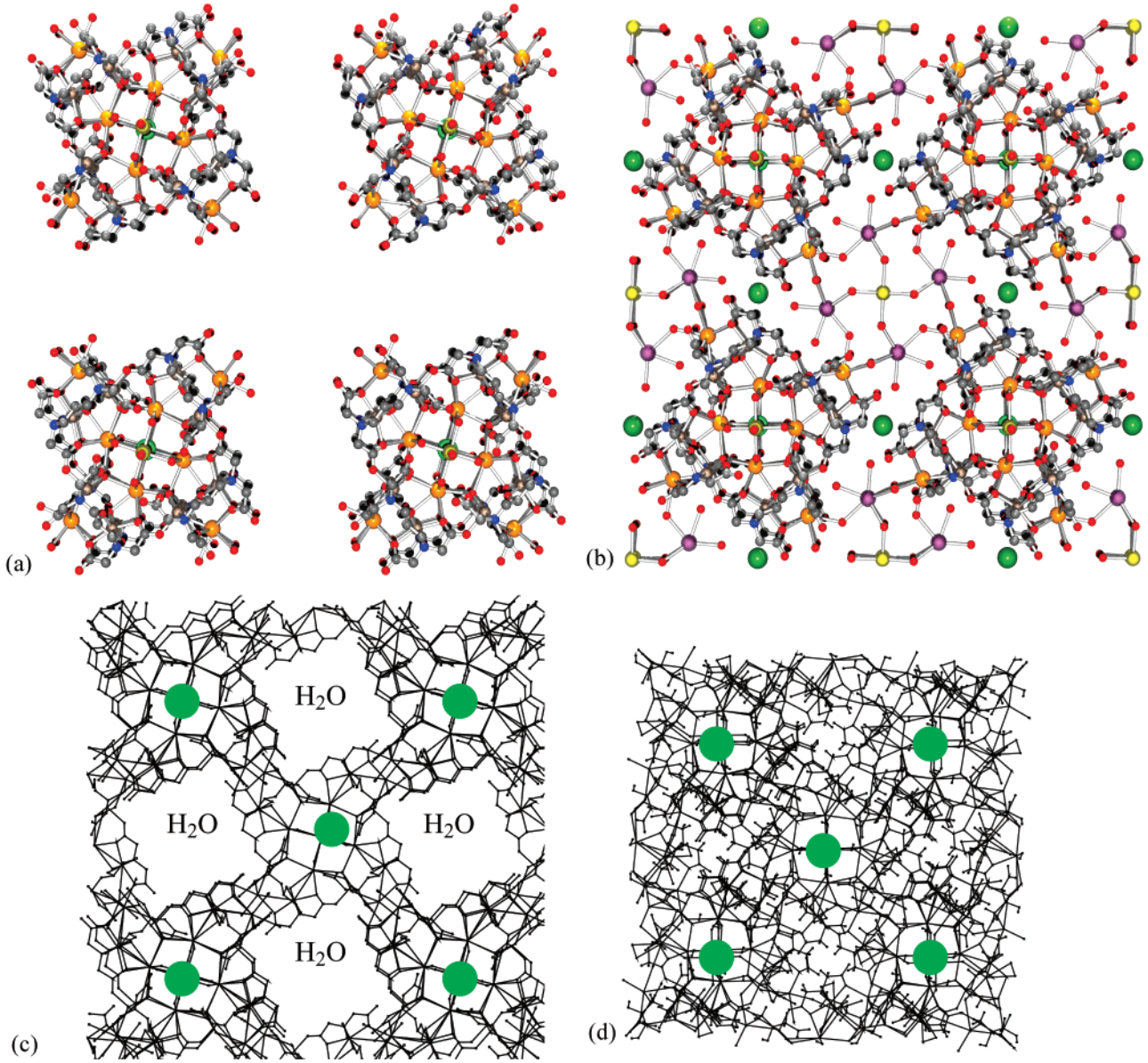

Figure 4. a, b. Packing diagrams of a single layer of Mn_{16} units present in the unit cells of two phases, viewed in projection along the *c* axis. The atoms are colored following the color codes of Figure 1. The two structural types, **1** and **2**, have similar unit cells (see Table 1). (a) Structure-type **1**: **1a**−**c**. The interstitial water molecules have been omitted. (b) Structure-type **2**: **2a** and **b**. Figure 4c, d. Packing diagrams of the two phases, viewed along the *c* axis. In comparison with Figure 4a and b, a Mn_{16} unit that belongs to another layer is projected in the center. Water molecules have been omitted. The circles mark the center of the Mn_{16} units. The different sizes of the diagrams, drawn on scale, result from the differences between the interaggregate distances of the two phases. (c) **1a**−**c**. (d) **2a** and **2b**. The extra (relative to **1a**, **1b**, and **1c**) Ba^{2+}, Na^+, and Cl^- ions and water molecules, depicted in Figure 4b, have also been omitted.

shaped distribution, have a mean of 3.150 and a median of 3.159 Å. For organic O−H···Cl^- units, O···Cl distances ranging from 2.9 to 3.3 Å are considered to indicate H-bonding.[15] The corresponding 3.10 ± 0.01 Å distances observed for the D_2O phases are within the range of both organic and inorganic molecules, actually equal to, or slightly below their average, respectively. Thus, the literature data, in addition to the X-ray location and refinement of the deuteron, support the hydrogen-bonded chloride motif of Figure 3b.

Unlike the deuterons in **2**, the hydroxo protons of **1a**−**c** were not detected via X-ray diffraction, but the presence of a H-bonded water in the H_2O structures at the location of Cl^- in the D_2O structures suggests that there are at least four μ-OH groups ($m = 4$ in Table 1), as shown in Figure 2a. Charge considerations based upon the XAS data[11] suggest an even higher number, namely eight protons per each Mn_{16} unit, perhaps located on all eight μ-oxo bridges ($m = 8$ in Table 1). Interestingly, a Mn_4−calcium−chloride ions motif, perhaps related to the topology of Figure 2b, is present at the active site of the oxygen-evolving complex of Photosystem II.[16,17,18] The above motifs, which show both alkaline and hydrogen-bonded chloride ions, self-assemble in the presence of NaCl and Na_2CO_3. In their absence, only Mn_4−alkaline-earth aggregates[19] are formed regardless of the isotope used.

As a direct result of isotopic substitution, the extra Ba^{2+}, Na^+ and Cl^- ions of the D_2O phase link the previously isolated Mn_{16} subunits to form supramolecular aggregates, as shown in the partial packing diagrams of Figure 4a, b.

The Mn_{16} units, which are linked by light water, become part of a polymeric solid upon change to heavy water. Thus, the structural influence of the isotopic exchange makes itself felt not at the stage of the building of the molecular Mn_{16} units, which contain mainly covalent bonds, but at their periphery, i.e. in the interaggregate space, where hydrogen bonding predominates. Stated differently, the heavy isotopomer favors supramolecular aggregation by inclusion of additional, hydrated Na^+, Ba^{2+}, and Cl^- ions. The simultaneous higher degree of overall hydration and shrinkage of the unit cell volumes upon isotope substitution (see Table 1 and Figure 2) is due to the presence of these ions. In essence, the Mn_{16} building blocks are relatively isolated, or as part of an extended solid depending on whether H_2O or D_2O is used during crystallization. This observation highlights the structural importance of hydrogen-bonding differences between the two hydrogen isotopes and suggests a way to rationally link aggregates in supramolecular assemblies using D_2O.

Notably, depending upon the isotope used, channels may be open or closed within the solid-state assemblies, as illustrated in Figure 4c, d.

In Figure 4c, d, the two phases are scaled to exhibit the same dimensions for their Mn_{16} units, consistent with the X-ray results and Figure 2. The picture of the H_2O phase is larger relative to the D_2O phase, as per their $a = b = 25.0 \pm 0.4$ and $a = b = 20.90 \pm 0.1$ Å unit cell dimensions, respectively. The D_2O structure is strikingly more compact and does not exhibit the water-lined channels of the H_2O phase. Thus, in some cases, it might be possible to tune the porosity of a solid by changing the water isotopomer used in its synthesis, a potential advantage for sorption and catalytic applications.

The above structural differences have magnetic consequences as well. The variable-temperature magnetic susceptibility profile for the H_2O and D_2O complexes[20] is significantly different, Figure 5.

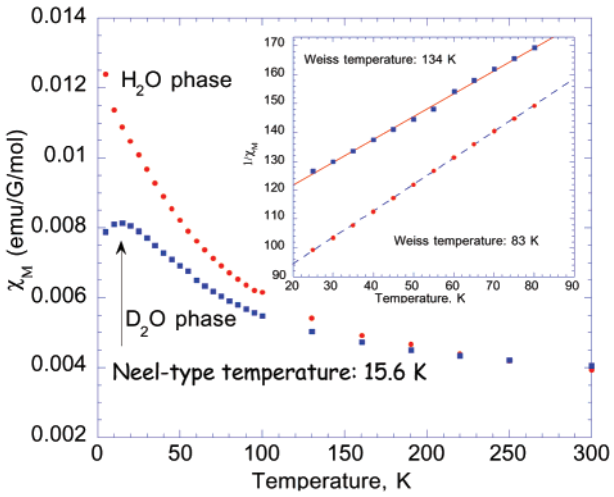

Figure 5. Temperature-dependent variation of the magnetic susceptibility of **1a** and **2b**. Inset: Currie−Weiss plots and linear fitting.

Both phases are characterized by overall antiferromagnetic behavior, with total spin states approaching $S_T = 0$ at 6 K. The magnitude of the couplings between 20 and 80 K, estimated from Curie−Weiss plots (Figure 5, inset) yields Weiss temperatures of 83 and 134 K for **1a** and **2b**, respectively. Deviations from linearity are noticed above and below this range. These data suggest that the Mn ions in the D_2O phase are more strongly coupled. The soft maximum observed at 15.6 K only for **2a** is reminiscent of a Néel point. The different magnetic properties of **1** and **2** might be related to the more compact association between Mn_{16} subunits in **2** (Figure 4c, d) or possibly to differences in the magnetic coupling within individual Mn_{16} units. The latter may be the result of small variations in the individual Mn oxidation states or bond lengths (Figure 2a, b). As noted above, the Mn_{16} units in **1** and **2** are structurally very similar, thus precluding the firm establishment of small oxidation-state level differences via X-ray diffraction. If the differences in Mn oxidation states are real, it follows that changing the water isotopomer results in an electronic change at the molecular level, i.e., Mn_{16}-complex level, in addition to influencing their aggregation. This phenomenon may be due to the presence of extra ions in the D_2O phase.

2. Isotope Effects on Iron Oxide Phases Formed in Nonconfined (Solution) Environments. The above deuterium-induced change in the composition, supramolecular assembly and magnetic properties of the manganese aggregates prompted us to seek whether similar effects might be manifested in the polymerization of simple iron salts. The isotope effect was

(13) Cambridge Crystallographic Database, April 2001 release.
(14) Allinger, N. L. *Adv. Phys. Org. Chem.* **1976**, *13*, 2.
(15) Jeffrey, G. A.; Saenger, W. *Hydrogen Bonding in Biological Structures*; Springer-Verlag: New York, 1994.
(16) Only the three most recent reviews are listed. Robblee, J. H.; Cinco, R. M.; Yachandra, V. K. *Biochim. Biophys. Acta* **2001**, *1503*, 7.
(17) Ananyev, G. M.; Zaltsman, L.; Vasko, C.; Dismukes, G. C. *Biochim. Biophys. Acta* **2001**, *1503*, 52.
(18) Vrettos, J. S.; Limburg, J.; Brudvig, G. W. *Biochim. Biophys. Acta* **2001**, *1503*, 229.
(19) Gorun, S. M.; Stibrany, R. T.; Lillo, A. *Inorg. Chem.* **1998**, *37*, 836.

(20) The microcrystalline complexes were measured in a constant field of 10000*G* using a Quantum Design SQUID MPMS 5S.

studied both in pure inorganic (unconstrained or nonconfined) environments and, as discussed in the next section, in the biologically constrained environment of the protein shell of ferritin.

The oxidation and hydrolysis of iron at physiological pH can be represented by reaction 1, where $Fe(OH)_{3(s)}$ corresponds to the various hydrated phases of iron(III) that are precursors to more stable minerals. Subsequent dehydration reactions lead to a variety of iron oxide mineral phases through reaction 2:[21,22]

$$4Fe^{2+}_{(aq)} + O_{2(g)} + 10H_2O_{(l)} \rightarrow 4Fe(OH)_{3(s)} + 8H^+ \quad (1)$$

$$Fe(OH)_{3(s)} \rightarrow FeOOH_{(s)}, Fe_2O_{3(s)} + nH_2O \quad (2)$$

As a proof-of-principle experiment, ferrous sulfate was aerobically oxidized and hydrolyzed for 48 h in both H_2O and 99.9% D_2O (Experimental Section). The 4.2 K Mössbauer spectra[23] of the lyophilized precipitates from H_2O (**3**, Figure 6a) and D_2O (**4**, Figure 6b), reveal that both samples contain a mixture of α-Fe_2O_3 (hematite) and γ-Fe_2O_3 (maghemite), *but in different ratios*. The γ spinel is more favored in the D_2O phase compared to the H_2O phase, $46 \pm 6\%$ vs $28 \pm 9\%$. Each sample was prepared in triplicate over the course of a year; a greater abundance of the γ spinel in the D_2O sample was observed in every instance.

Although there is limited information available on the detailed mechanism of metal oxo/hydroxo group formation during hydrolytic polymerization of iron oxides, some useful observations can be made. Since neither of the oxide phases contain protons, the observed isotope effect on the relative amounts of α- and γ-Fe_2O_3 must influence the formation of reaction precursors, "$Fe(OH)_3$" (reaction 1), and the subsequent processes that lead to oxides (reaction 2). The reaction precursors undoubtedly contain a significant number of hydrogen bonds that may be affected by the isotopic exchange. The "aging" process of iron(III) hydroxides, which results in the reduction in the number of hydrogen bonds through dehydration of the solid, can take days or longer to complete.[21,22] In contrast, the time scale of O−H/O−D exchange in aqueous solutions is much shorter compared to that of polymerization (aggregation), the kinetics of H-exchange between tritiated water and α- and β-FeOOH crystals formally obeying a diffusion controlled law.[24,25] Equilibrium isotope effects (as opposed to the classical kinetic one) are maximized in ionic media, in the presence of exchangeable protons.[26] Taken together with the small difference in the O−H vs O−D bond strength, the above observations suggest that oligomerization processes at room temperature are expected to be only minimally affected by the classical deuterium kinetic isotope effect, but are largely dominated by thermodynamics. Thus, it is likely that the isotope effect observed here on the mineral distribution between α-Fe_2O_3 and γ-Fe_2O_3 is a thermodynamic one rather than a kinetic one. Unlike the effect of H/D exchange on the manganese aggregate, the iron oxide products obtained from the oxidation, hydrolysis and dehydration reactions have the same chemical composition, but different phase ratios.

3. Isotope Effects on Iron Core Formation in Ferritin. The isotope effect seen in the inorganic iron polymerization raises the question whether an isotope effect would be observed in iron biomineralization within the confined cavity of the iron storage protein ferritin. Biologically controlled mineralization[7−10,27] results in well-defined iron particles in the nanoscale domain and/or simple crystals of magnetic oxides, such as magnetite, which in the case of magnetotactic bacteria are single magnetic domains.[7,8] Unlike solutions, the confined environment of apoferritin cavity exhibits a well-defined topology of carboxylic groups that bind iron.[9] This hollow space thus provides nucleation sites that direct the growth but limit the size of the metal aggregates. As a result, the hydrolytic polymerization process is controlled to a certain extent, certainly to a larger degree relative to the same process that occurs in nonconfined (solution) environments. Importantly, the magnetic phases form in water around pH = 7 and thus are susceptible to water isotope changes.

To probe the existence of an isotope effect in biomineralization, iron was deposited at a level of 1500 Fe/protein in horse spleen apoferritin using Fe(II) and O_2 as the oxidant, in either H_2O (sample **5**) or D_2O (sample **6**) buffers (Experimental

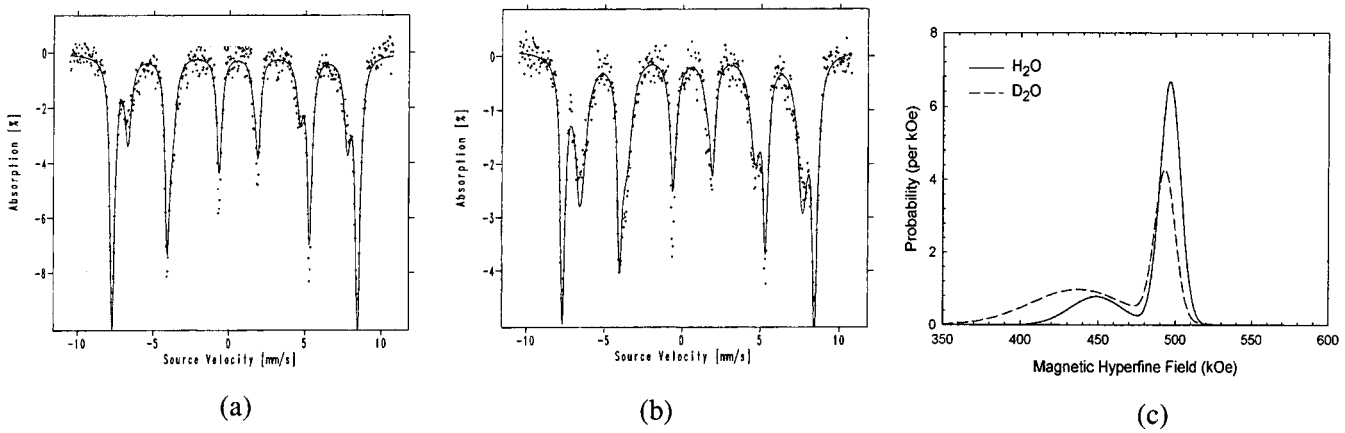

Figure 6. Typical 4.2 K Mössbauer spectra of iron oxides from (a) H_2O and (b) D_2O. Each spectrum is comprised of the superposition of two magnetic subspectra. The results are the averages of six independently prepared samples. The majority component (outer absorption sixplet) is identified as bulk phase α-Fe_2O_3, while the minority component (inner absorption sixplet) as nanoscale size, superparamagnetic γ-Fe_2O_3. Fitted Mössbauer parameters: (a) outer spectrum, isomer shift, $\delta = 0.49$ mm/s, quadrupolar perturbation, $\epsilon = -0.24$ mm/s, magnetic hyperfine field, $H_{hf} = 500$ kOe, relative absorption area, $A = 72 \pm 9\%$. Inner spectrum, $\delta = 0.50$ mm/s, $\epsilon = 0$ mm/s, $H_{hf} = 447$ kOe, $A = 28 \pm 9\%$. (b) Outer spectrum, $\delta = 0.50$ mm/s, $\epsilon = -0.25$ mm/s, $H_{hf} = 498$ kOe, $A = 54 \pm 6\%$, inner spectrum, $\delta = 0.52$ mm/s, $\epsilon = 0$ mm/s, $H_{hf} = 439$ kOe, $A = 46 \pm 6\%$. (c) Magnetic hyperfine field distributions corresponding to the theoretical fits.

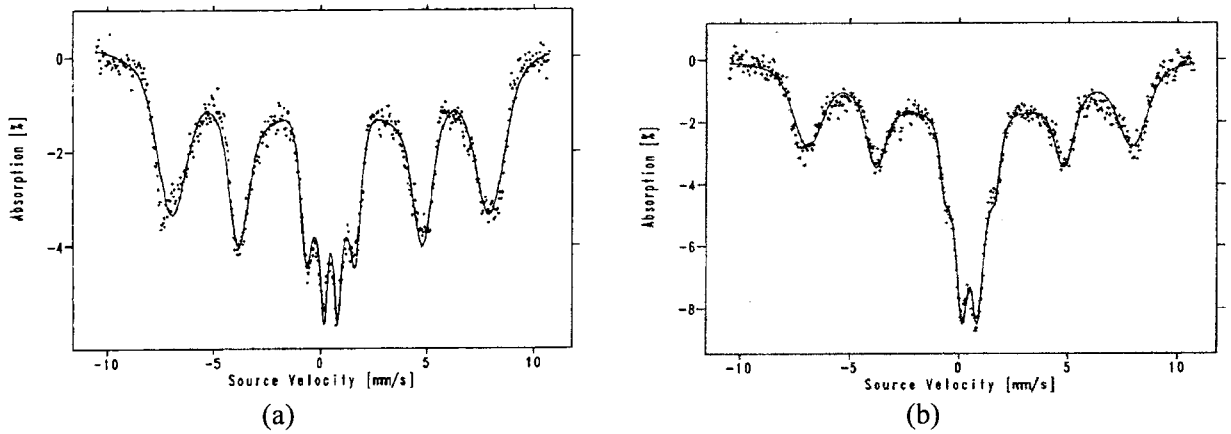

Figure 7. Mössbauer data for iron loaded superparamagnetic ferritins at 30 K. (a) **5**, H_2O ferritin. (b) **6**, D_2O ferritin. Each spectrum is comprised of the superposition of a quadrupole doublet (at the center of the spectrum) and a broad magnetic sixplet. Fitted Mössbauer parameters[23] are (a) central doublet, isomer shift $\delta = 0.485$ mm/s, quadrupole splitting $\Delta E_Q = 0.61$ mm/s, relative absorption area $A = 12\%$, magnetic sixplet (fit to a magnetic field distribution), $\delta = 0.485$ mm/s, average hyperfine field $H_{hf} = 460$ kOe, $A = 88\%$. (b) Central doublet, $\delta = 0.48$ mm/s, $\Delta E_Q = 0.68$ mm/s, $A = 21\%$, magnetic sixplet, $\delta = 0.485$ mm/s, $H_{hf} = 460$ kOe, $A = 79\%$.

Section). Figure 7 shows the Mössbauer spectra of the resulting ferritin samples.

The spectra are typical of the ferrihydrite-like "$5Fe_2O_3 \bullet 9H_2O$" core of ferritin.[9] The temperature dependence of the spectra shows classical superparamagnetic behavior with blocking temperatures of 40 and 60 K for the D_2O and H_2O samples, respectively (Figure 8).

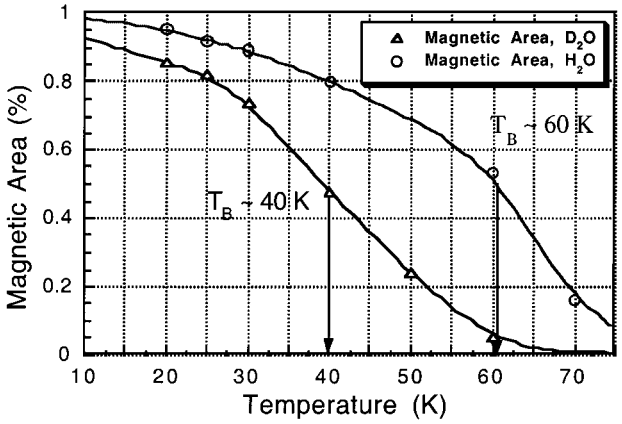

Figure 8. Temperature dependence of the magnetic fraction of the Mössbauer spectra for H_2O and D_2O ferritins. The solid line is drawn through the experimental points to aid the eye. The blocking temperatures, T_B, are indicated by arrows.

In this instance, the isotope effect is reflected in the 20 K lower blocking temperature for the D_2O sample, a property due to the lower magnetic anisotropy energy for this sample, i.e., less crystallinity, and/or a smaller average core particle diameter than for the H_2O sample. While the replacement of H_2O with D_2O in the mineral core is expected to influence its properties, the role of the protein ferroxidase and nucleation sites in mineralization is probably affected as well since the pK_a's of protein functional groups are higher in D_2O than in H_2O by 0.3 to 0.8 units.[28] Thus it seems likely that biomineralization may be influenced by H/D exchange at a number of levels.

In the three solid-state systems examined here, several isotope-specific thermodynamic parameters might contribute to the observed divergence of phases, changes in phase ratios or morphologies when samples are prepared in light and heavy water. For example, the collective hydrogen-bond strength differences may favor the incorporation of additional hydrated cations and anions in the manganese complex prepared in D_2O. Elevated pK_a's for metal ion hydrolysis in D_2O, as is well-known for the acid dissociation of other functional groups,[28] might translate into different degrees of protonation of metal-bonded-oxo/hydroxo groups near neutral pH (pD). Different degrees of ionization in H_2O and D_2O solutions may be reflected in the ratio of μ-oxo/μ-hydroxo groups of the manganese aggregates, in the dissimilar results of the slow iron hydroxide aging process to produce differing ratios of hematite (α-Fe_2O_3) and maghemite (γ-Fe_2O_3), and in the properties of ferritin cores.

Conclusions and Outlook

The three types of experiments described here indicate that changing the hydrogen isotope can have a significant effect on the structural and physical properties of metal aggregates formed in aqueous solutions. Varying the H-bonding, the pH and perhaps other parameters by replacing H_2O with D_2O (without the compositional perturbation by the addition non-hydrogen ions) may provide opportunities in the future for obtaining inorganic and biological metal aggregates with new properties. Perhaps even the synthesis and phase characteristics of lacunar solids and nanosized materials, at the molecule−solid-state interface,[29] might be affected by this simple isotope substitution, as suggested by the supramolecular aggregation of Mn_{16} units and the differences observed in the case of iron in oxides and ferritin cores. Phase ratios and materials morphologies might be affected in certain cases as well. Deuteration might also have consequences, beyond the classical kinetic isotope effect, upon

(21) Flynn, C. M., Jr. *Chem. Rev.* **1984**, *84*, 31.
(22) Schneider W.; Schywn, B. In *Aquatic Surface Chemistry: Chemical Processes at the Particle−Water Interface*; Stumm, W., Ed.; Wiley: New York, 1987; pp 167−196.
(23) Greenwood N. N.; Gibb, T. C. *Mössbauer Spectroscopy*; Chapman and Hall: London, 1971.
(24) Gallagher, K. J.; Phillips, D. N. *Trans. Faraday Soc.* **1968**, *64*, 785.
(25) Gallagher, K. J.; Phillips, D. N. *Chimia* **1969**, *23*, 465.
(26) Heinzinger, K.; Weston, R. E., Jr. *J. Phys. Chem.* **1964**, *68*, 744.
(27) Mann, S. *J. Inorg. Biochem.* **1986**, *28*, 363.
(28) Li, N. C.; Tang, P.; Mathur, R. *J. Phys. Chem.* **1961**, *65*, 1074.
(29) Papaefthymiou, G. C. *Phys. Rev. B.* **1992**, *46*, 10366.

the long-range ordering of biomolecules, electron transfer, magnetic exchange interactions (as shown for manganese), and possibly, the proper function of pK_a-sensitive enzymes. In future work, related chemical and biological systems will be studied to determine whether the initial observations reported here have general applicability in the production of new materials.

Experimental Section

Manganese Complexes. The ligand L (H_5dhpta) was purchased from Aldrich and used without purification. Deuterium peroxide (D_2O_2) was prepared by vacuum distilling 30 mL of 30% H_2O_2, adding 15 mL of 99.9% D_2O, and redistilling to one-third of the volume. This procedure was repeated three additional times and then 20 mL of D_2O was added to D_2O_2 solution. *Caution: concentrated or anhydrous hydrogen peroxide is potentially explosive.* $Ba(OH)_2•8H_2O$ and $Ba(OD)_2•8D_2O$ were prepared by recrystallizing $Ba(OH)_2•H_2O$ from H_2O or 99.9% D_2O, respectively. $Ba_2(Hdhpta)•3H_2O$: recrystallized $Ba(OH)_2•8H_2O$ (4.622 g, 1.465×10^{-2} mol) was added to a suspension of H_5dhpta (2.363 g, 7.332×10^{-3} mol) in 50 mL of deionized water. The mixture became clear and then deposited a white precipitate, which was collected by filtration, washed with diethyl ether, and dried. 95% yield. A similar procedure using D_2O yields $Ba_2(Ddhpta)•3D_2O$.

Preparation of Mn_{16} complexes **1a**, **1b**, **1c**, **2a**, and **2b**. Anhydrous manganous acetate, $Mn(OAc)_2$, (0.163 g, 9.42×10^{-4} mol) was added to a mixture of $Ba_2(Hdhpta)•3H_2O$ or $Ba_2(Ddhpta)•3D_2O$ (0.3 g, 4.7×10^{-4} mol) and NaCl (1.00 g) in 15 mL of degassed H_2O or D_2O. Next, 3.13 mL of an aqueous $Ba(OH)_2$ solution (0.5 equiv vs $Ba_2(Hdhpta)•3H_2O$) and 1.8 mL of H_2O_2 (or their deuterated analogues) were added sequentially, generating a brown color. The solutions were placed in contact with 0.025 g solid Na_2CO_3. X-ray quality single crystals form after several days. Correct metal ions ratio analysis. The full analysis is also correct, but the number of water molecules is subject to some error, as reflected by the X-ray structural determinations and facile water loss during handling. The full analysis of **1b**, for example, formulated as $Mn_{16}O_{8-m}(OH)_m(CO_3)_4L_8Ba_8Na_2Cl•53H_2O$ indicates that 15 water molecules have been lost. Anal Calcd for $C_{92}H_{188}N_{16}O_{130}Na_2ClMn_{16}Ba_8$ ($m = 0$): C, 19.53; H, 3.35; N, 3.96; Cl, 0.63. Found: C, 19.67; H, 3.17; N, 3.94; Cl, 0.74. Statistically indistinguishable values are obtained for $m = 4$.

X-ray Analysis. The structures were obtained from single-crystal X-ray data using conventional direct methods and difference Fourier techniques, followed by least-squares refinement of atomic coordinates and thermal parameters. All non-hydrogen atoms were refined anisotropically (see the Supporting Information).

Preparation of Fe_2O_3 Oxides 3 and 4. Solid $FeSO_4•7H_2O$ (0.248 mg) was dissolved in 0.5 mL H_2O (or D_2O) and the pH (or pD = pH meter reading + 0.4, standardized against H_2O buffer reading) brought to 2.0 with NaOH (or NaOD) while stirring. This solution was added to 4 mL of 0.2 M MOPS buffer in H_2O (or D_2O) while stirring. After 2 days, the reddish-brown precipitate was collected and washed with H_2O (or D_2O) and lyophilized. Contact with atmospheric moisture was avoided during the procedure involving D_2O.

Preparation of Ferritins 5 and 6. Deuterated (>99.99%) horse spleen ferritin was prepared by repeated (6X) ultrafiltration of 15 μM apoprotein against deuterated 0.2 M MOPS buffer, pD = 7.5 over a period of 2 days. The protein was diluted to 2 μM concentration in deuterated pD = 7.5 buffer to give a volume of 6 mL. To this solution was added 15 increments of 24 μL 0.049 M $^{57}FeSO_4$ in D_2O, pD = 2, at intervals of at least 1/2 h over a period of 2 days to give a total iron loading of 1500 ^{57}Fe/protein. The MOPS buffer was then replaced by 99.99% D_2O using ultrafiltration and the protein sample lyophilized. The protein sample in H_2O was prepared similarly at pH 7.5 using normal buffers.

Acknowledgment. C. Day, V. Day, N. Brooks, V. Young, Jr., and A. Viescas and R. Stibrany are thanked for initial X-ray structural data and skillful experimental assistance, respectively. J. Abernathy (Cambridge Isotopes Laboratory) is thanked for a generous donation of D_2O. This work was supported in part by Brown University start-up funds and Cambridge Isotopes Laboratory (S.M.G.), by NIH grant R37 GM20194 (N.D.C.), and NSF grant DMR-0074537 (G.C.P.).

Supporting Information Available: X-ray data collection details, figures, and crystallographic tables for **1a**, **1b**, **1c**, **2a**, **2a′**, and **2b**. This material is available free of charge via the Internet at http://pubs.acs.org.

JA011447Q